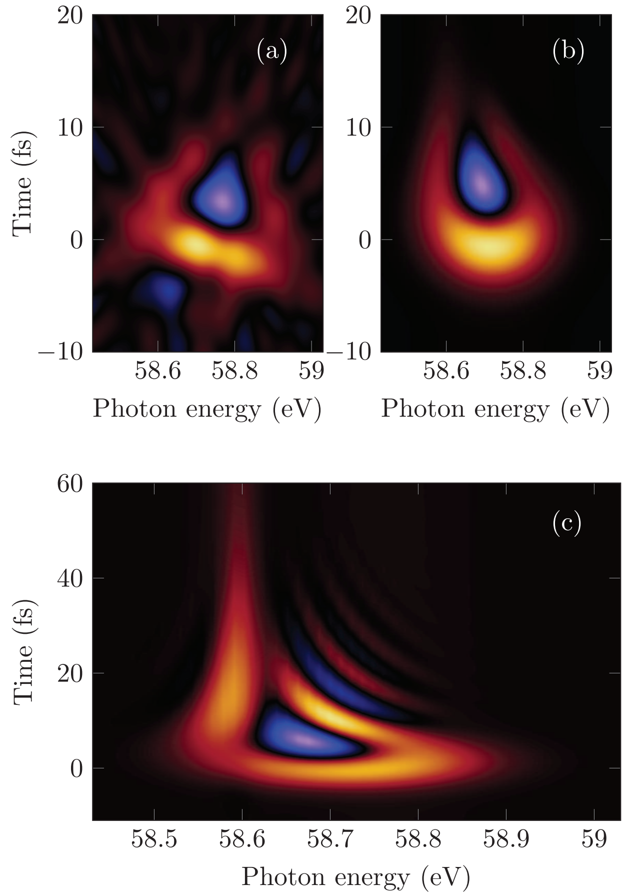

Figure 8. Wigner distribution. (a) Experimental WD, (b) simulated WD using the finite pulse model with experimental parameters for the XUV and IR pulses, (c) simulated WD using the finite pulse model with experimental parameters for the XUV and a 10nm broad IR pulse.

are defined as:

$$W_D(E_\mathrm{f},t) = \int \delta(t+\frac{\tau}{2})\delta(t-\frac{\tau}{2})\,\mathrm{e}^{iE_\mathrm{f}\tau/\hbar}\,\mathrm{d}\tau \tag{13}$$

$$W_I(E_\mathrm{f},t) = i\frac{\Gamma}{2\hbar}\int (i-q)\mathrm{e}^{-(iE_\Phi/\hbar+\Gamma/2\hbar)\left(t+\frac{\tau}{2}\right)}\Theta\left(t+\frac{\tau}{2}\right)$$
$$\times\,(q+i)\mathrm{e}^{(iE_\Phi/\hbar-\Gamma/2\hbar)\left(t-\frac{\tau}{2}\right)}\Theta\left(t-\frac{\tau}{2}\right)\mathrm{e}^{iE_\mathrm{f}\tau/\hbar}\,\mathrm{d}\tau \tag{14}$$

$$W_{ID}(E_\mathrm{f},t) = \int \mathrm{d}\tau\,\delta(t+\frac{\tau}{2})\;i\frac{\Gamma}{2\hbar}(q+i)$$
$$\times\exp\left[\left(\frac{iE_\Phi}{\hbar}-\frac{\Gamma}{2\hbar}\right)\left(t-\frac{\tau}{2}\right)\right]\Theta\left(t-\frac{\tau}{2}\right)\mathrm{e}^{iE_\mathrm{f}\tau/\hbar} \tag{15}$$

The calculation of W_D is straightforward and gives $W_D = \delta(t)$. For W_I we get:

$$W_I = \frac{\Gamma^2}{2\hbar}(q^2+1)\exp\left(-\frac{\Gamma t}{\hbar}\right)\frac{\sin\left(2\frac{E_\mathrm{f}-E_\Phi}{\hbar}t\right)}{E_\mathrm{f}-E_\Phi} \tag{16}$$

Finally we get that

$$2\mathrm{Re}(W_{ID}) = -\frac{\Gamma}{\hbar}e^{-\Gamma t/\hbar}\,\Theta(t)$$
$$\times\left[q\sin\left(\frac{2(E_\mathrm{f}-E_\Phi)t}{\hbar}\right)+\cos\left(\frac{2(E_\mathrm{f}-E_\Phi)t}{\hbar}\right)\right] \tag{17}$$

The first term, W_D, corresponds to the direct transition to the continuum and, once convolved with the spectrum of the ionizing pulse, results in a large feature observed at $t = 0$ fs. The second term W_I, describes the decay of the autoionizing state in the continuum, at the energy E_Φ. Finally the last term results from the interference of both contributions and leads to oscillations with an hyperbolic shape observed in figure 8(c).

6. Conclusion

In summary, we have presented calculations and measurements of the amplitude and phase of EWPs emitted through the sp2$^+$ and sp3$^+$ Fano resonances in helium using the Rainbow RABBIT technique. We discussed aspects that may affect these spectrally-resolved measurements, in particular the spectrometer resolution and the finite pulse effects. The retrieved amplitude and phase were then used to fully characterize the wave packets in the time-frequency space which allowed us to disentangle the dynamics associated with the different ionization channels. The sensitivity of the technique can be improved by using harmonics with a broad spectral width providing a locally smooth amplitude variation and allowing the measurement of fast changes in the ionization cross section. In addition, the combination of long dressing pulses to minimize finite-pulse effects with photoelectron spectrometers with high resolving power (combined with deconvolution techniques) can greatly increase the spectral resolution of the RABBIT technique. Time-frequency representations offer a powerful tool to characterize EWP emitted close to resonances where strong electron correlations lead to significant time-frequency couplings. In particular, we have shown that the WD can potentially provide unique insights into electron correlation during autoionization. This could be extended to the study of photoionization in more complex systems such as molecules of biological interest and solids. Another potential application of the WD is the complete tomographic reconstruction of partially coherent ultrashort pulses in the XUV and X-ray range [45].

Acknowledgments

This research was supported by the European Research Council (Advanced grant PALP), the Swedish Research Council, the Knut and Alice Wallenberg Foundation, Sweden, the Laserlab-Europe EU-H2020 654148, the EU H2020-MSCA-ITN-MEDEA-641789, the ANR-15-CE30-0001-CIMBAAD, ANR-